Moroccan Journal of Chemistry
ISSN: 2351-812X
http://revues.imist.ma/?journal=morjchem&page=login
El Hadrami & al. / Mor. J. Chem. 8 N°3 (2020) 615-626

Structural evolution and impact on the compressive strength of fly ash-based geopolymers

A. El Hadrami[a,*], S. Ojala[b], E. M. Chatir[a,c], J. Assaoui[d], R. Brahmi[c]

[(a)] Laboratory of Physico-Chemistry of Materials (LPCM), Chemistry Department, Faculty of Sciences, University of Chouaïb Doukkali, BP 20, 24000 El Jadida, Morocco.
[(b)] Faculty of Technology, Environmental and Chemical Engineering, University of Oulu, P. O. Box 4300, FI-90014 Oulu, Finland.
[(c)] Laboratory of Coordination and Analytical Chemistry (LCCA) Department of Chemistry, Faculty of Sciences, University of Chouaïb Doukkali, BP 20, 24000 El Jadida, Morocco.
[(d)] Department of Chemistry, Faculty of Sciences, University of Chouaïb Doukkali, BP 20, 24000 El Jadida, Morocco.

** Corresponding author:*
elhadrami.ab@gmail.com
Received 18 May 2020,
Revised 25 Jun 2020,
Accepted 27 Jun 2020

Abstract

This paper concentrates on valorization of the fly ash originating from thermal power plant by alkaline activation. Structural and textural characterization of raw material and prepared geopolymers was carried out. The used raw material belonged to Class F according to ASTM C618-05 and it was mainly composed of quartz, mullite, hematite and calcite, that coexisted with hydroxy-sodalite in final geopolymers. The proportion of the hydroxy-sodalite phase increased with the concentration of the activating agent. During geopolymerization, structural changes appeared including the incorporation of aluminum into the silicate network leading to their crosslinking. Textural characterization showed that the material became more compact during the geopolymerization process, which in agreement with the increase of hydroxy-sodalite phase. These changes lead to an increase of mechanical strength of geopolymers.

Keywords: *Fly ash, Inorganic waste, Alkali-activation, Valorization, Compressive strength.*

1. Introduction

Annually, the industry generates millions of tons of waste and the growing production presents a serious problem. Thus, industrial production faces increasingly stringent environmental requirements. The power plants are the sources of large quantities of solid waste, which are typically landfilled. In Morocco, these power plants produce about 570,000 tons of fly ash annually [1], which poses a threat to the water, soil and plants. Indeed, when settling on plants, fly ash prevents transpiration and photosynthesis of the plants. They affect negatively to soil quality, since they are basic and poor in nitrogen and phosphorus. On the other hand, the global cement industry generates up to 4.0 billion tons of CO_2 per year [2]. In fact, this industry is responsible for nearly 5% of the world's total CO_2 emissions [3], thus contributing to global warming through the greenhouse effect. In order to solve these two problems, several studies have been carried out focusing generally on the recycling the fly ash by geopolymerization and using the geopolymer as an alternative to the Portland cement, to store toxic and radioactive waste, and in manufacturing molds for plastics and aluminum alloys [4–8]. The geopolymerization procedure is based on an alkaline activation of solid precursors containing aluminosilicates. The geopolymers have typically SiO_2/Al_2O_3 molar ratio between 3 and 3.8 [8,9]. The advantage of the geopolymerization is that the activation proceeds at low temperature and generate a much lower level of CO_2 emissions compared to the traditional cement production. Geopolymerization of fly ash involves a chemical reaction between the different aluminosilicate oxides with highly alkaline solutions producing oligomers by polymerizing the Si-O-Si and Si-O-Al bonds. Then, a polycondensation of oligomers gives rise to a three-dimensional alumino-silicate networks [5,8]. The entire process is supported by thermal agitation of molecules using heating at temperatures between 40 and 80 °C during 48 hours [5,10,11]. The compressive strength development of the geopolymers using fly ash as the only silica and alumina source is highly dependent on both the synthesis conditions and the characteristics of the raw material subjected to the activation process.The aim of this work is the valorization of waste from thermal power plant by developing a basic geopolymer based-material having a good mechanical properties that can be used in the construction applications... The structural evolution as a function of NaOH concentration and its influence on the final properties of the geopolymer namely mechanical properties are studied and discussed.

2. Materials and methods

2.1. Preparation of geopolymers

The fly ash (lablled FA) used in this work was collected from the thermal power plant located in Jorf Lasfar/El Jadida, Morocco. The geopolymers (named as “GeoPX” X meaning the concentration of NaOH) were prepared by activating dried fly ash with different concentrations of NaOH solution (2.5. 5. 7.5. 10 and 12 M). During the preparation the fly ash was mixed with NaOH solution respecting a solid/liquid ratio of 8/3 [mass (g) / volume (mL)] to obtain a consistent paste. Resulting paste was kneaded with a spatula for 5 minutes, poured into aluminum molds and placed in an oven heated at 60 °C for 48 hours.

2.2. Characterization

The particle size distribution of raw material was determined by laser granulometry using water as a dispersing agent in MASTERSIZER 2000 MALVERN device.

The chemical composition was determined by X-ray Fluorescence spectroscopy using a wave dispersion spectrometer (WD-XRF) type Axios. The loss of ignition (LOI) was determined by taking a ground mass and introducing it into the muffle furnace operating at 1000 °C for 12 hours. The diffractograms were obtained using a BRUKER D8 X-ray diffractometer operating at 45KV / 35mA and equipped with CuKα radiation (λKα = 1.54056 Å). The data were

collected over a 2Θ range of 10-70 ° using a step size of 0.02. Morphological characteristics were examined by a field emission Scanning Electron Microscopy ZEISS ULTRA plus coupled with EDS analysis. The sample was fixed with double adhesive tape before coating the sample with gold. The infrared absorption spectra were recorded using a Fourier transformed spectrometer (Nicolet iS10 Thermo Fisher) equipped with Attenuated Total Reflection (ATR) mounting in the wave number range between 525 and 4000 cm^{-1} with a resolution of 2 cm^{-1} and with 30 scans. The Raman spectra were obtained using a Timegated 532 Raman instrument (Timegate Inc.) equipped with sub-nanosecond (100 ps) pulsed laser excitation source (532 nm) coupled with time-gated single photon counting array detector (C-MOS/SPAD). Such arrangement is capable of avoiding fluorescence interference. Thermal behavior was examined by thermogravimetric (TG) and differential thermal analysis (DTA) on the Shimadzu DTG-60 h model with a measurement accuracy of 0.001 mg and a heating rate of 1 °C / min. The specific surface areas and pore volumes of fly ash and geopolymers were determined from the isotherms of nitrogen physisorption at 77 °K using an ASAP 2020 Micrometrics apparatus. After hardening and demolding the samples in a cylindrical shape were kept in the air at room temperature and then subjected to the compressive test at 7 and 28 days using a MTS Criterion electromechanical press (Model 43).

3. Results and discussion

3.1. Characterization of raw material

The particle size distribution of a raw material is one of the important physical characteristics, which strongly influences the reactivity of the material. In fact, a large part of the reaction takes place at the particle-liquid interface. The finer the particles, the larger is the contact surface and thus the fly ash is more reactive [12,13]. The examination of particle size of used fly ash, shown in Figure 1, reveals a bimodal distribution centered at 10 and 100 µm of diameter. 50% of particles have a diameter less than 57 µm and about 90% of particles present the diameter less than 231 µm.

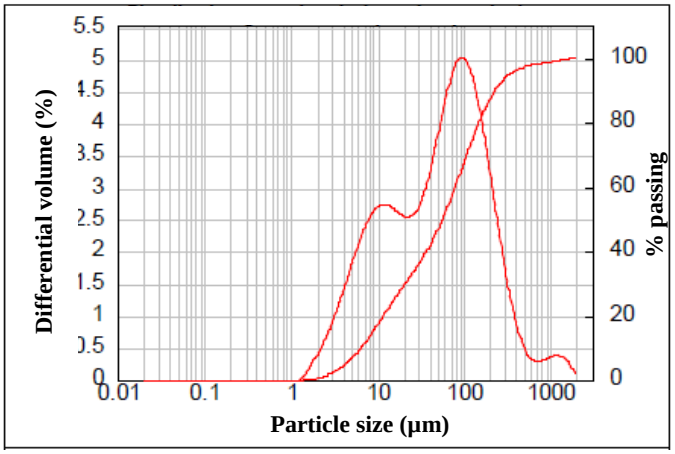

Figure 1. Particle size distribution of raw material.

The composition of fly ash was determined by XRF and calculated in the form of most probable oxides (Table 1). The main constituents of fly ash are SiO_2 (43%), Al_2O_3 (19.8%) and Fe_2O_3 (14.3%). Calcium oxide, magnesium oxide, titanium oxide, sulphur, phosphorus and potassium are also present in quantities of less than 4%. As the sum of the SiO_2. Al_2O_3 and Fe_2O_3 percentages is in the order of 77% and a calcium oxide content is less than 8%, the fly ash can be classified in class F in accordance with the requirements described in ASTM specification N° C618-05 [14]. The SiO_2/Al_2O_3 molar ratio is about 3.6, which suggests an easy geopolymerization [12] and good compressive strength [9].

The loss of ignition (LOI) is 11.8 % (Table 1) can be attributed to the unburned coal resulting from the combustion process and to decomposition of carbonates present in the fly ash. This value is higher than, those found in other studies [6,15–17]. On the other hand, the TG-DTA- analysis under air showed, that the exothermic decomposition of fly ash started at around 600 °C and the total mass loss is around 10%, which is close to that previously observed during calcination (Figure 2).

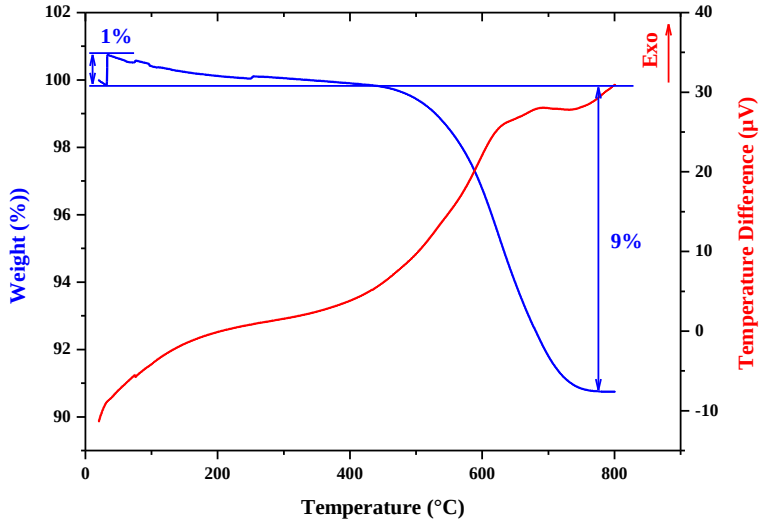

Figure 2. DTA and TG analysis of fly ash.

The X-ray diffractogram of the as-received fly ash (Figure 3) reveals the presence of several crystalline phases, including quartz (SiO_2. JCPDS 01-083-0539), mullite ($Al_6Si_2O_{13}$. JCPDS 00-015-0776), calcite ($CaCO_3$. JCPDS 01-072-1937) and hematite (Fe_2O_3. JCPDS 01-073-0603). The major phases identified are in agreement with the results of elemental analyses by XRF. In addition, we note the presence of an amorphous phase represented by a large hump located between 18 and 36 ° (2θ) in agreement with the literature [13,15,18].

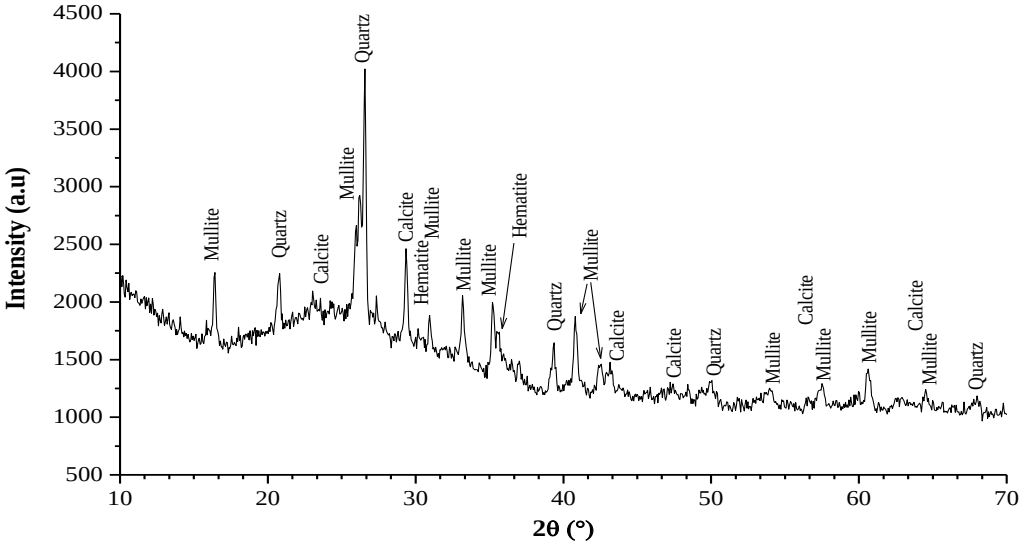

Figure 3. X-ray pattern of fly ash as-received.

3.2. Characterization of geopolymers

The composition of the geopolymers prepared by activation with different concentrations of NaOH were determined by X-ray fluorescence (Table 1). The geopolymers activated by NaOH 2.5 and 5 M have almost the same composition as the raw material, but the content of SiO_2 and Al_2O_3 decrease by increasing the concentration of NaOH. This

decrease coincides with the increase of the Na content indicating the formation of a sodium-containing phase, which can be confirmed by XRD. Note that the mass balance was completed by LOI, since carbon and water are not detected by the X Ray Fluorescence. The XRD patterns of the geopolymers show that the crystalline phases quartz, mullite, hematite are still present and the intensities of their peaks vary very little. This reflects the fact that they are not attacked by the activating solution and therefore do not participate in the geopolymerization reaction. In addition, a new phase corresponding to the hydroxy-sodalite $Na_8(AlSiO_4)_6(OH)_2.2H_2O$ appears gradually while calcite phase disappears (Figure. 4) with increasing of the concentration of NaOH. The formation of the hydroxy-sodalite phase is in agreement with XRF results that showed the increase of sodium amount of geopolymer starting from a NaOH concentration of 7.5 M (Table 1). As the calcium content remains practically constant in the geopolymers, it is very likely that the phase containing it is in the amorphous part. Hydroxy-sodalite phase forming network consists of SiO_4 and AlO_4 tetrahedrons [19]. The incorporation of Al in tetrahedral sites leads to a strong network reticulation, which can influence the mechanical properties. Through these results, we can conclude that geopolymerization process leads to a structural rearrangement mainly at the expense of the amorphous phases.

Table 1. *Chemical composition of fly ash and geopolymers calculated as representative oxides from the XRF analysis.*

Oxides	**FA**	**GeoP2.5M**	**GeoP5M**	**GeoP7.5M**	**GeoP10M**	**GeoP12M**
SiO_2	42.7	41.4	40.9	33.6	32.1	32.0
Al_2O_3	19.7	18.4	17.6	15.1	14.3	13.5
Fe_2O_3	14.2	14.9	13.7	15.4	14.4	14.6
K_2O	3.9	3.6	3.4	3.8	3.2	3.1
CaO	1.9	3.3	2.4	2.7	2.2	2.1
TiO_2	2.7	2.5	2.3	2.7	2.2	2.2
P_2O_5	1.3	1.9	0.9	1.3	0.9	1.0
SO_3	1.2	1.2	0.8	0.8	0.8	0.6
MgO	0.6	0.5	0.4	0.4	0.4	0.2
Na_2O	0.0	0.0	0.0	4.1	7.8	6.1
LOI	11.8	12.2	17.6	20.05	21.7	24.2
Total	100	99.9	100	99.95	100	99.6
SiO_2 + Al_2O_3 + Fe_2O_3	76.6	74.7	72.2	64.1	60.8	60.1
SiO_2/Al_2O_3 (molar ratio)	3.7	3.8	3.9	3.8	3.8	4

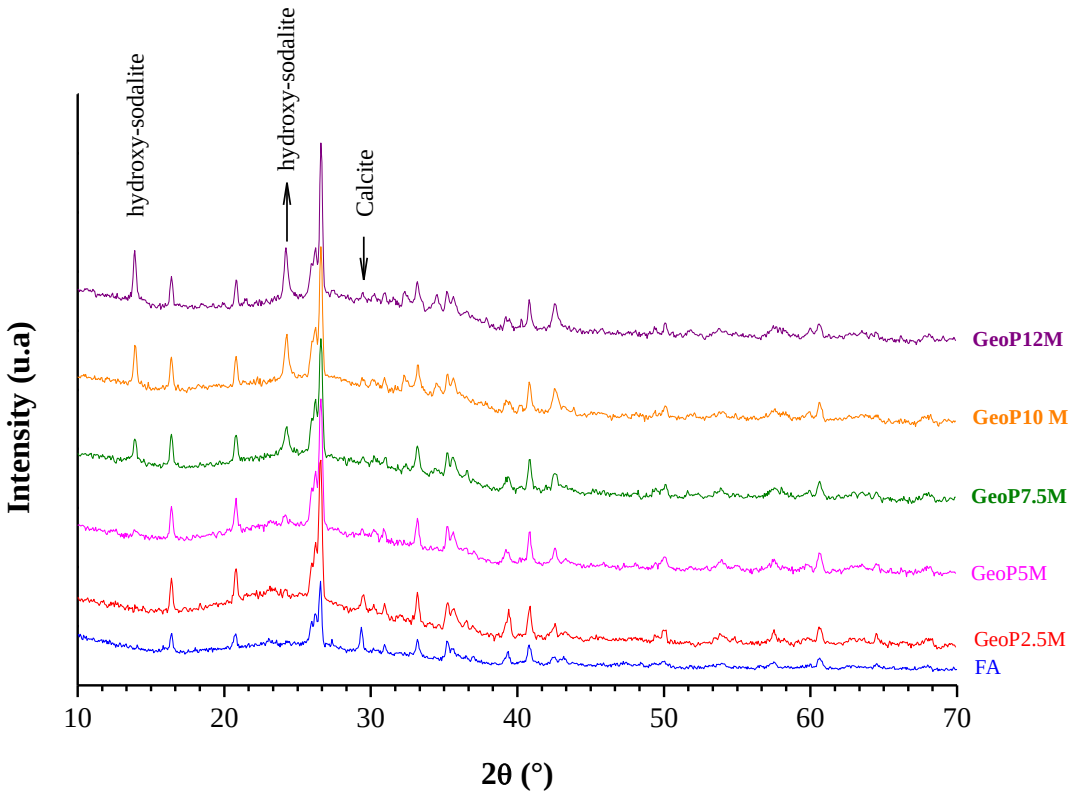

Figure 4. X-ray diffractograms of fly ash and geopolymers treated with different concentrations of NaOH.

The infrared spectra recorded in the wave number range between 525 and 4000 cm^{-1} are shown in Figure 5. The infrared spectrum of fly ash is similar to the spectra represented in the literature [20–22]. Absorption bands at approximately 1020, 890, 770, 730, 680 and 590 cm^{-1} have been identified. The strong absorption band located at 1020 cm^{-1} is attributed to the asymmetric vibration mode ν_{as} Si—O—Si and ν_{as} Si—O—Al [20]. The two bands located at 770, 730 and 680 cm^{-1} are assigned respectively to the symmetrical vibration mode ν_s Si—O—Si, ν_s Si—O—Al and bending deformation mode δSi—O—Si [6,23]. The shoulder marked at 890 cm^{-1} corresponds to the Si—O—H deformation mode [21,23]. Other authors have attributed this shoulder to the vibration of the Si-O-M groups (with M = Ca, Na or Fe) [4]. Finally, the band observed at 590 cm^{-1} is due to the deformation mode of the Si-O-Al link [7]. This Si-O-Al bond is associated with the presence of aluminum at the octahedral sites in the mullite [24]. The geopolymerization appears in the infra-red spectra as the appearance of new bands located at 3400, 1644 and 1450 cm^{-1}. The first two bands are attributed respectively to the stretching vibration and deformation of the O-H bond [25] and the third band is related to the appearance of the CO_3^{2-} group resulting from the reaction of CO_2 present in the air and residual Na [21]. In addition, the main band located at 1020 cm^{-1} for fly ash moves to a lower frequency (960 cm^{-1}) after geopolymerization. This is explained by the aluminium incorporation into the silicate network by adopting tetrahedral coordination and an increase in the number of non-bridging oxygens in the silicon tetrahedral [6]. Indeed, Si—O—Al bonds have smaller angles than Si—O—Si bonds thus leading the signal to appear at a lower frequency. Overall, this shift towards lower frequency is the consequence of a formation of large molecular structure and strong network reticulation. Note also that the intensity of the band located at 770 cm^{-1} decreases markedly, which is attributed to the destruction of Si—O—Si bonds in amorphous phase. This change in the IR spectra is in good agreement with the X-ray diffraction results, which showing the formation of hydroxy-sodalite where the aluminium is located in tetrahedral sites. Raman results are presented in Figure 6. Generally, in the case of silicate materials, the bands between 1200 and 800 cm^{-1} are associated with Si─O stretching vibrations in SiO_4 tetrahedra [26]. In this interval four main bands can be observed at 1200 cm^{-1}, 1100 –1050 cm^{-1}, 1000–950 cm^{-1}, 900 cm^{-1} and 850 cm^{-1} corresponding to the symmetrical elongation vibrations of silicate tetrahedra with four (Q^4), three (Q^3), two (Q^2), one (Q^1) and zero (Q^0) bridging oxygens (BO), respectively[26]. The bands observed in the low frequency zone (700 to

300 cm^{-1}) are attributed to the modes of stretching vibration in the links T─O─T (T = Si or Al) [26,27]. The measured Raman spectra of fly ash show the presence of a very strong and thin peak at 455 cm^{-1}. This peak can be attributed to the symmetrical stretching vibration mode of the Si─O─Si link in quartz in accordance with the literature [28]. Two shoulders located at 490 cm^{-1} and 415 cm^{-1} are assigned respectively to the vibrations of oxygen in rings connecting 4 and 6 tetrahedra of TO_4 (T = Si or Al) in an amorphous phase [29]. The shoulder located at 350 cm^{-1} has been attributed to the deformation mode of the O─Si─O et O─Al─O links [30]. In the high frequency range (800-1200 cm^{-1}), the spectrum presents a very wide band with a medium to low intensity. Despite the overlaps, we can speak of two bands : one located at 830 cm^{-1} and the other at 1140 cm^{-1} respectively attributed to the mode of stretching vibration of the Si─O bond in the silicate tetrahedron at 4 non-bridging oxygen (Q^0) and the Si─O bond in the silicate tetrahedron with 4 bridging oxygen (Q^4) [6]. Activation of fly ash changes the Raman spectra. In the low-frequency region, a low intensity band between 550 and 570 cm^{-1} appears. This band is probably associated with formation of Al─O─Al bridges [27]. In addition, the peak at 830 cm^{-1} increases in intensity as it moves towards the higher frequency reflecting the formation of Q^1 entities to the detriment of Q^0 entities. At the same time, a new broad band centered at 1030 cm^{-1} due to the Si─O asymmetric vibration mode has appeared suggesting the presence of Q^2 and Q^3 entities [6,29]. In the fly ash and geopolymer spectra the peaks observed around 1340 and 1570 cm^{-1} were attributed to the bonds of vitreous carbon and graphite (G) still present in the fly ash even after coal combustion process or to the appearance of the CO_3^{2-} group generated during the reaction of CO_2 in the air and residual sodium.

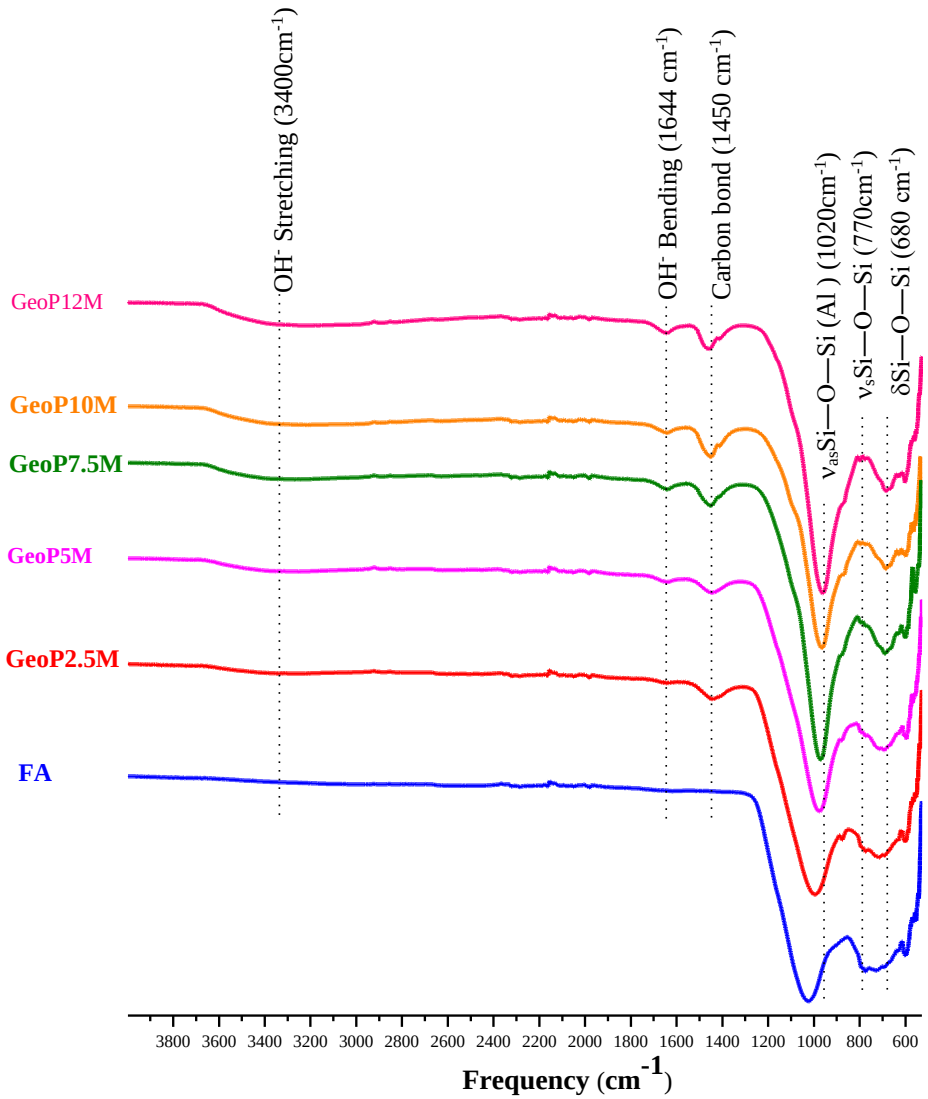

Figure 5. Infrared spectrum of raw fly ash and geopolymers.

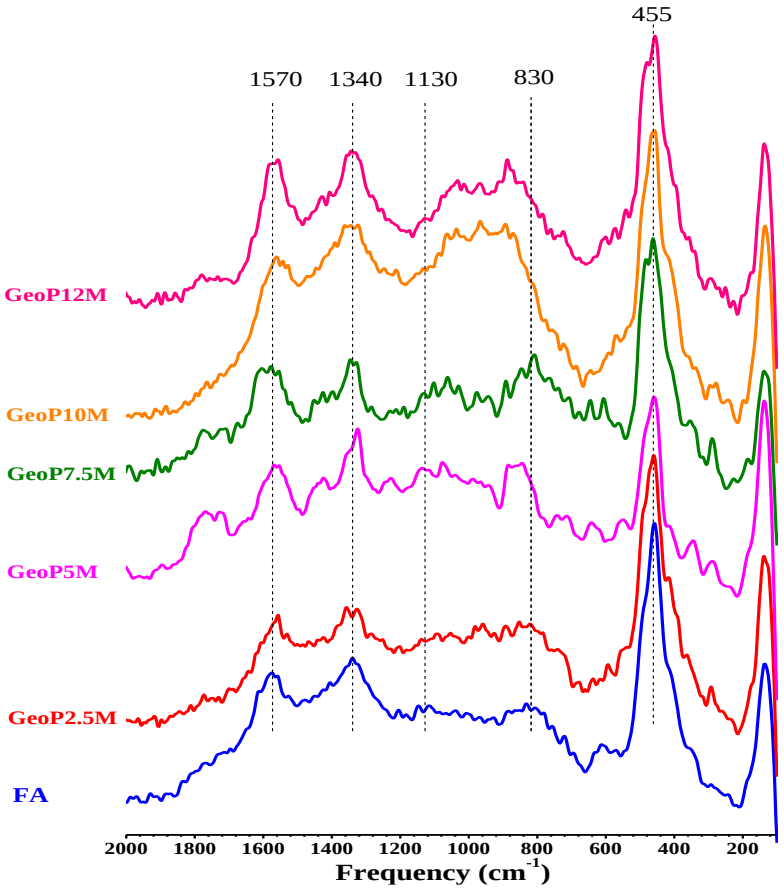

Figure 6. Raman spectra of raw fly ash and geopolymers.

The thermal stability of the prepared geoplymers was followed by TG-DTA analysis (Figure 7). All geopolymers have the same decomposition profile presenting two mass losses accompanied by two endothermic and exothermic peaks. The first mass loss region ranges from 100 to around 400 °C, and becomes stronger with the concentration of the activating agent (NaOH). This implies an increase in the proportion of the hydroxy-sodalite phase. The mass loss in the mentioned temperature range is 2 wt-% for the GeoP2.5M and around 6 wt-% for the GeoP12M sample. These are related to the loss of water present in the structure of the hydroxy-sodalite, which in agreement with Schipper et al. [31]. The formed anhydrous hydroxy-sodalite phase $Na_8(AlSiO_4)_6(OH)_2$ then decomposes at 747 °C into an anhydrous cargenite Na[A1SiO$_4$]. 1/6 Na_2O [32]. In addition, the mass loss above 400 °C can be also related to the decomposition of sodium carbonates generated by the reaction of residual sodium and carbonates in the atmosphere [33]. As a conclusion, the prepared geopolymers are thermally stable up to 400 °C, which makes them interesting candidates for construction applications.

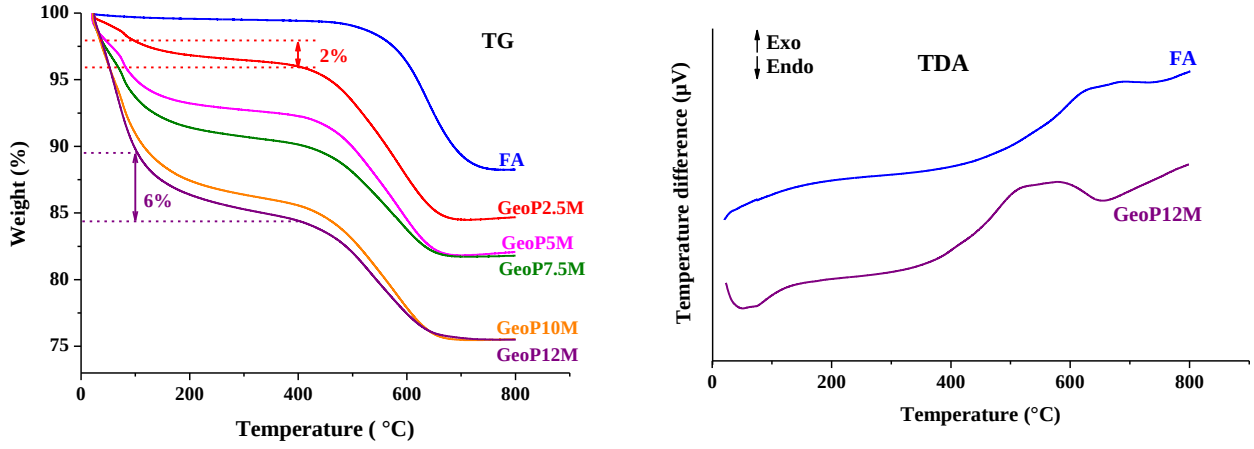

Figure 7. TDA and TGA curves for geopolymers compared to crude fly ash.

SEM micrographs of as-received fly ash and geopolymers are compared in Figure 8. The results show an overview of the microstructure of the fly ash having a porous sponge-like structure made up of particles of spherical shape with different sizes (0.1 to 3 µm). The geopolymerization leads to a notable change in the microstructure due to the total or partial dissolution of the spherical particles and formation of a new microstructure, which becomes more pronounced with the higher NaOH concentration. In addition, the micrograph shows the persistence of many particles, which are not attacked or only partially attacked by the activating solution indicating non-complete geopolymerization. This leads to formation of an aluminosilicate gel covering the surface of the fly ash particles, which results in the encapsulation of Si and Al and the prevention of new particle formation [6]. In fact, GeoP12M sample highlights the presence of different shapes of crystals and a gel coating on the particles making the structure more compact. The surfaces of all the materials studied are heterogeneous and developing lower porosities, which is typical for geopolymers based on fly ash. Therefore, the BET specific surface areas of fly ash and geopolymers are very low, around 3 $m^2.g^{-1}$.

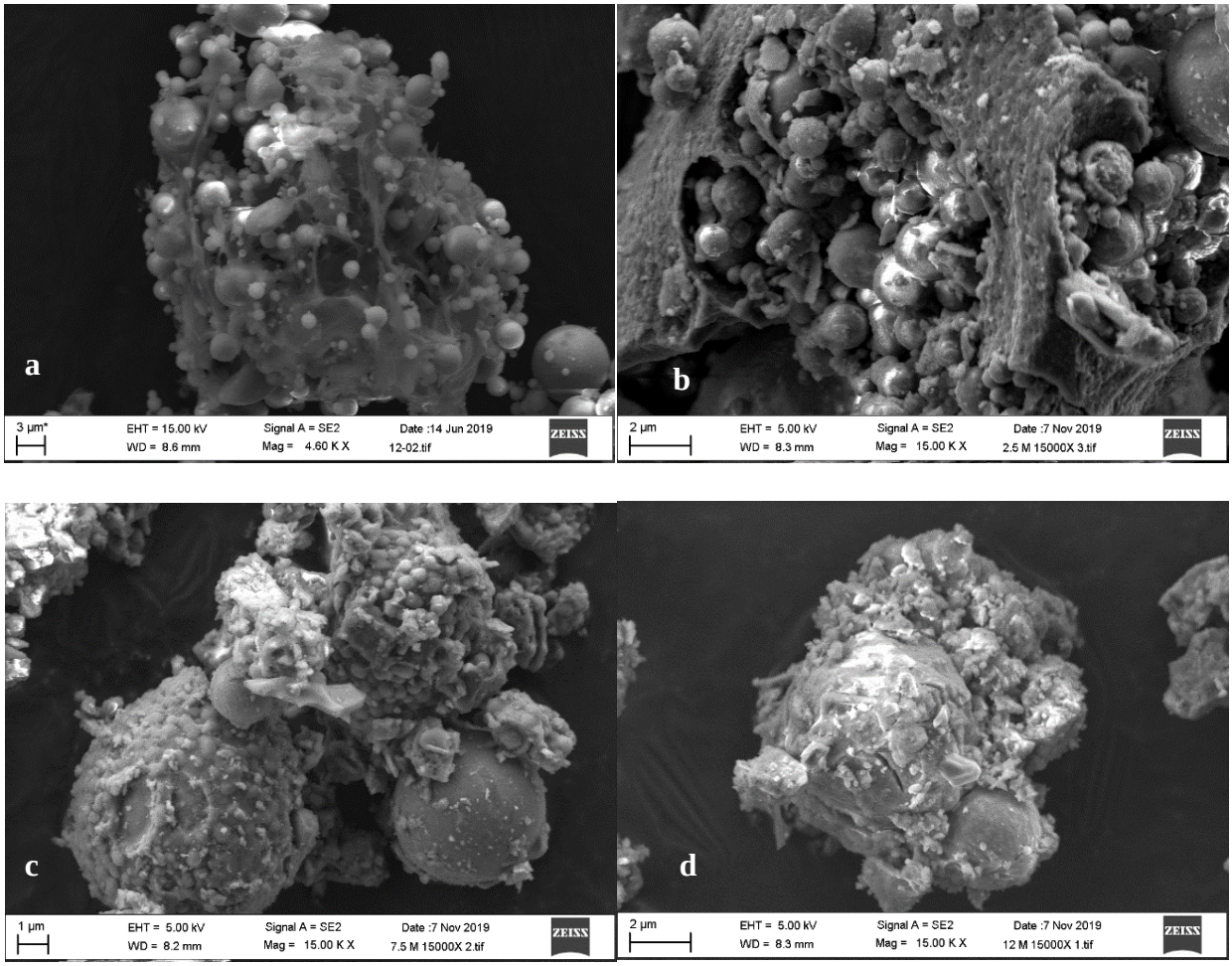

Figure 8. SEM micrograph of geopolymers of a: As-received Fly Ash; b GeoP 2.5 M; c: GeoP 7.5 M; d: GeoP 12 M.

The EDS mapping of Al, Si and Na in the geopolymers (Figure 9) show that they are well dispersed and closely linked. On the other hand, the amount of Na increases with the increase of the concentration of NaOH (Table 2), which is in good agreement with the increase in the hydroxy-sodalite phase. In spite of the difference in chemical composition that can be noted in comparison with the X-ray fluorescence, the EDS results confirm the classification of the used fly ash in class F with SiO_2/Al_2O_3 molar ratio around 3.6.

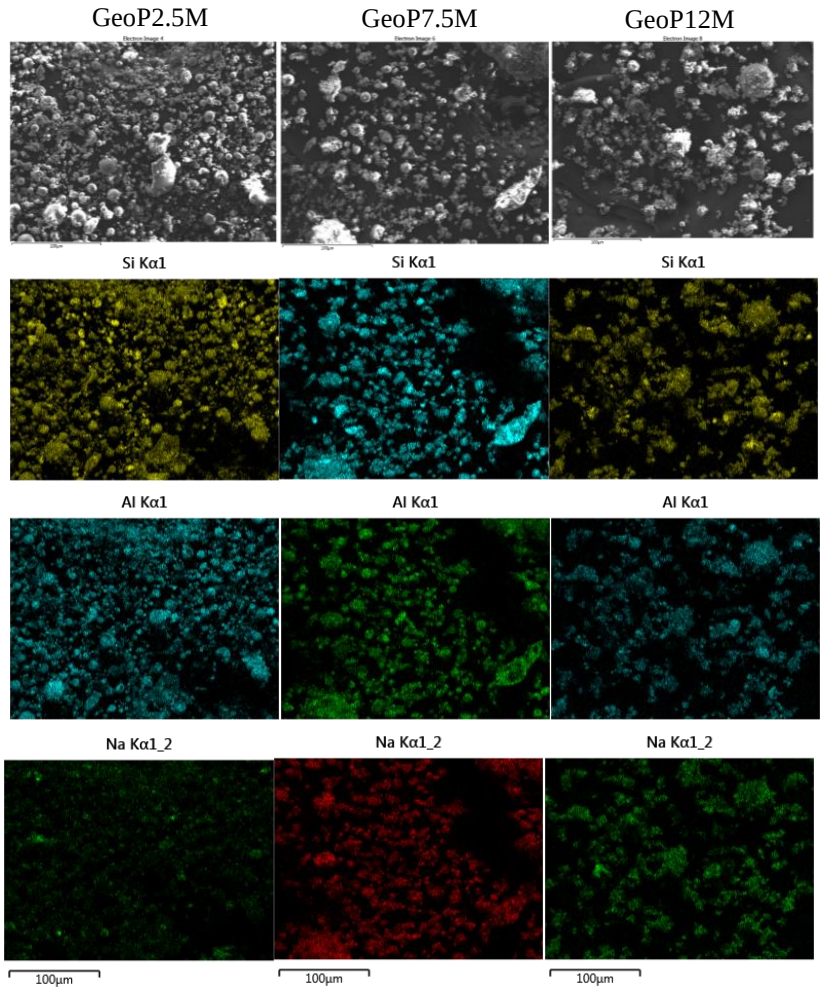

Figure 9. Mapping of the main elements of the geopolymers.

Table 2. Chemical composition of fly ash and its geopolymers in oxide form based on EDS analysis.

Oxide	Molar %			
	FA	GeoP2.5 M	GeoP7.5 M	GeoP12 M
SiO_2	66.42	65.94	58.03	52.99
Al_2O_3	18.51	17.01	16.75	15.17
Fe_2O_3	3.04	4.07	3.32	4.68
K_2O	2.34	2.40	2.25	1.92
CaO	2.45	2.67	2.05	3.11
SO_3	2.65	0.00	0.51	0.00
TiO_2	1.50	1.58	1.78	0.70
MgO	1.90	1.14	0.90	0.74
Na_2O	0.99	5.19	14.40	20.69
Total	100.00	100.00	100.00	100.00
SiO_2/Al_2O_3	3.59	3.88	3.46	3.49
Na_2O/ Al_2O_3	0.05	0.30	0.86	1.37

The mechanical properties of the geopolymers were assessed by determining the compressive strength. Figure 10 shows an overview of the variation of compressive strength versus the concentration of the activating solution for the different geopolymers aged 7 and 28 days. It is clearly established that the compressive strength increases with the

increase in the concentration of the activating agent, and therefore by the increase in the proportion of the hydroxy-sodalite phase. In fact, the high concentration of OH^- ions promotes dissolution of particles and aluminosilicate gel formation, and thus the formation of hydroxy-sodalite, as observed by XRD and FTIR (formation of Si-O-Al). GeoP12M sample develops the best compressive strength (32 MPa) after 28 days. Taking into account the molar ratios of SiO_2/Al_2O_3 and Na_2O/Al_2O_3 that are around 3.6 and 1.37 for the GeoP12M sample, the result of the compressive strength is predictable and are in good agreement with the literature [9,34].

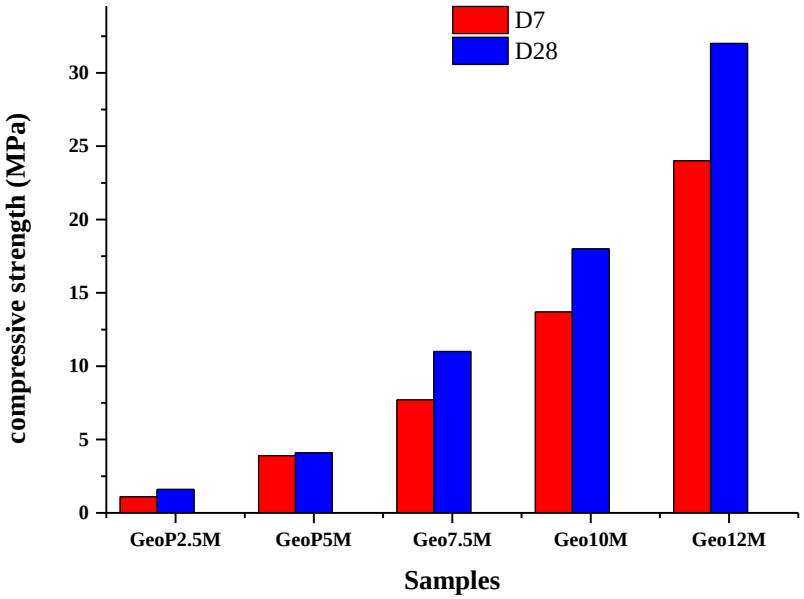

Figure 10. Compressive strength of the geopolymers.

4. Conclusion

The aim of this work was to valorize fly ash originating from a Moroccan thermal power plant. To reach this goal we proposed their geopolymerization using NaOH solution as the sole alkaline activating agent with different concentrations at 60 °C. The results showed that this low-energy geopolymerization process allowed the transformation of the waste into sustainable products with suitable properties for building applications. The X-ray diffraction study showed that the fly ash is mainly composed of quartz, mullite, calcite and hematite in addition to an amorphous phase. The fly ash was classified in the Class F based on its chemical composition. For NaOH concentrations above 5 M the geopolymerization was reflected by the disappearance of calcite and the appearance of hydroxy-sodalite phase, which increases with the concentration of NaOH. Vibrational spectroscopy showed that aluminum is tetracoordinated and confirmed the structural changes by the formation of Si-O-Al and the presence of Q^2 and Q^3 entities, when NaOH concentration increases. The SEM revealed the formation of a gel coating on the particles, which makes the structure more compact, in particular for GeoP12M. Mechanical strength is improved by higher concentrations of NaOH, reaching a value of 32 MPa for GeOP12M, in agreement with the increase of the ratio of the hydroxy-sodalite phase in the geopolymer. Geopolymers prepared from fly ash develop interesting structural, textural and mechanical properties which make them promising materials for use in mortar and concrete.

References

[1] K. Bazzar, M.R. Bouatiaoui, A.H. Alaoui, *Int. J. Eng. Sci. Innov. Technol.* 2 (2013) 663–671.

[2] I. Phummiphan, S. Horpibulsuk, R. Rachan, A. Arulrajah, S.L. Shen, P. Chindaprasirt, *J. Hazard. Mater.* 341 (2018) 257–267.

[3] B. Nematollahi, J. Sanjayan, F.U.A. Shaikh, *Ceram. Int. 41* (2015) 5696–5704.

[4] Z. Zhang, H. Wang, J.L. Provis, J. Sustain. *Cem. Mater.* 1 (2012) 154–166.

[5] E. ul Haq, S.K. Padmanabhan, A. Licciulli, *Ceram. Int.* 40 (2014) 2965–2971.

[6] N. Böke, G.D. Birch, S.M. Nyale, L.F. Petrik, *Constr. Build. Mater.* 75 (2015) 189–199.

[7] C. Shi, A.F. Jiménez, A. Palomo, *Cem. Concr. Res.* 41 (2011) 750–763.

[8] J. Davidovits, *J. Thamal Anal.* 37 (1991) 1633–1656.

[9] P. De Silva, K. Sagoe-Crenstil, V. Sirivivatnanon, *Cem. Concr. Res.* 37 (2007) 512–518.

[10] S.K. Nath, S. Maitra, S. Mukherjee, S. Kumar, *Constr. Build. Mater. J.* 111 (2016) 758–765.

[11] E. Alvarez-Ayuso, X. Querol, F. Plana, A. Alastuey, N. Moreno, M. Izquierdo, O. Font, T. Moreno, S. Diez, E. Vazquez, M. Barra, *J. Hazard. Mater.* 154 (2008) 175–183.

[12] A.Fernández-Jiménez, A.Palomo, *Fuel.* 82 (2003) 2259–2265.

[13] E.I. Diaz, E.N. Allouche, S. Eklund, , *Fuel.* 89 (2010) 992–996.

[14] Standard Specification for Coal Fly Ash and Raw or Calcined Natural Pozzolan for Use in Concrete, (2005).

[15] A. M. Fernandez-Jiminez, E.E. Lachowski, A. Palomo, D. E.Macphee, *Cem. Concr. Compos.* 26 (2004) 1001–1006.

[16] A. Fernandez-Jimenez, D.. Macphee, E.. Lachowski, A. Palomo, *J. Nucl. Mater.* 346 (2005) 185–193.

[17] P. Nath, P.K. Sarker, *Constr. Build. Mater.* 130 (2017) 22–31.

[18] S.K. Nath, S. Kumar, *J. Non. Cryst. Solids.* 505 (2019) 241–251.

[19] I. Hassan, H.D. Grundy, *Acta Cryst.* C39 (1983) 3–5.

[20] S.M. Nyale, O.O. Babajide, G.D. Birch, N. Böke, L.F. Petrik, *Procedia Environ. Sci.* 18 (2013) 722–730.

[21] Z. Abdollahnejad, F. Pacheco-torgal, T. Félix, W. Tahri, J.B. Aguiar, *Constr. Build. Mater.* 80 (2015) 18–30.

[22] A. Palomo, M.W. Grutzeck, M.T. Blanco, *Cem. Concr. Res.* 29 (1999) 1323–1329.

[23] T. Uchino, T. Sakka, M. Iwasaki, *J. Am. Ceram. Soc.* 74 (1991) 306–313.

[24] A. Fernández-Jiménez, A. Palomo, *Microporous Mesoporous Mater.* 86 (2005) 207–214.

[25] H. Cheng-yong, L. Yun-ming, M. Mustafa, A. Bakri, *Sci. Rep.* 7 (2017) 1–11.

[26] P. Mcmillan, B. Piriou, R. Couty, *J. Chem. Phys.* 81 (1984) 4234–4236.

[27] D.R. Neuville, L. Cormier, D. Massiot, *Chem. Geol.* 229 (2006) 173–185.

[28] K.S. Sharma, J.F. Mammone, M.F. Nicol, *Nature.* 292 (1981) 140–141.

[29] S.K. Sharma, B. Simons, H.S. Yoder, *Am. Mineral.* 68 (1983) 1113–1125.

[30] K. Chah, B. Boizot, *Nucl. Instruments Methods Phys. Res. B.* 191 (2002) 337–341.

[31] D.J. Schppiper, T.W. Lathouwers, C.Z.V.A.N. Doorn, *J. Am. Ceram. Soc.* 56 (1973) 523–525.

[32] J. Felsche, S. Luger, *Thermochim. Acta.* 118 (1987) 35–55.

[33] P.N. Lemougna, K.J.D. Mackenzie, U.F.C. Melo, *Ceram. Int.* 37 (2011) 3011–3018.

[34] M. Kaur, J. Singh, M. Kaur, *Ceram. Int.* 44 (2018) 1534–1537.